ADVANCED MATERIALS TECHNOLOGIES
www.advmattechnol.de

Functional Polymer Nanocomposites by Gas Aggregation Cluster Source and Initiated Chemical Vapor Deposition

*Torge Hartig, Joschka Paulsen, Jonas Drewes, Asmaa T. Mohamed, Nasra F. Abdel Fattah, Cedric Hinrichs, Felix Pohl, Stefan Rehders, Ainura Aliyeva, Henning Wieker, Jörg Wiltfang, Salih Veziroglu, Samah A Loutfy, Oral Cenk Aktas, Alexander Vahl, Thomas Strunskus, Aydin Gülses, Amal Amin, Stefan Schröder, and Franz Faupel**

Functional metal-polymer nanocomposites are required for highly tailored surface properties and coatings. However, past approaches like cosputtering, physical evaporation, or plasma polymerization can not retain the functionality of the polymer matrix or produce tailored nanoparticles. A new kind of codeposition of nanocomposite polymer thin films is presented via the combination of a *gas aggregation cluster source (GAS)* and *initiated chemical vapor deposition (iCVD)* in a common GAS+iCVD vacuum system. iCVD delivers ultraprecise and defect-free polymer thin films on the nanoscale while a GAS creates nanoparticles that form in the gas phase and can be tuned in size and composition. Using the GAS+iCVD system, nanocomposites of well-defined Ag nanoparticles in a chemically intact PTFE polymer thin film are prepared. The deposited nanocomposite proved applicable in antibacterial applications by decreasing the colony-forming units of *Enterococcus faecalis* by 38%. Antiviral SARS-CoV-2 Spike-ACE-2 binding inhibition reaches 65% of pure silver nanoparticles. The nanocomposite improves the apoptotic gene expression for liver cancer cells compared to pure thin films. This new kind of codeposition paves the way for the fabrication of functional nanocomposite thin films combining the advantages of the iCVD polymer palette with a large variety of nanoparticles that can be prepared by GAS.

1. Introduction

Polymer-nanoparticle composites have long been used to combine the desired properties of structural or functional nanoparticles with a polymer matrix on the macroscale.[1,2]

On the nanoscale functional nanocomposite thin films are more complex to produce. To introduce new functionality to a polymer thin film, especially metal nanoparticles present advanced application possibilities. Wet chemical approaches to fabricate metal-polymer nanocomposites result in residual solvents, material defects, or agglomeration of particles which are often undesired in their advanced application areas. Gas phase approaches such as evaporation and plasma polymerization are currently state of the art but lack retention of polymer functionality, have a small molecular weight, and a limited polymer selection.[3] Cosputtering of metals

T. Hartig, J. Paulsen, J. Drewes, F. Pohl, S. Rehders, A. Aliyeva, S. Veziroglu, O. C. Aktas, A. Vahl, T. Strunskus, S. Schröder, F. Faupel
Chair for Multicomponent Materials
Department of Materials Science
Kiel University
24143 Kiel, Germany
E-mail: ff@tf.uni-kiel.de

A. T. Mohamed
Nanotechnology research center
The British University in Egypt
Cairo 11837, Egypt

N. F. A. Fattah, S. A Loutfy
Virology&Imunology Unit
Cancer Biology Department
National Cancer Institute
Cairo University
Cairo 11796, Egypt

C. Hinrichs, H. Wieker, J. Wiltfang, A. Gülses
Department of Oral and Maxillofacial Surgery
Campus Kiel
University Hospital of Schleswig-Holstein
24105 Kiel, Germany

S. Veziroglu, A. Vahl, T. Strunskus, S. Schröder, F. Faupel
Kiel Nano
Surface and Interface Science KiNSIS
Kiel University
24118 Kiel, Germany

A. Amin
Polymers and Pigments Department
Chemical Industries Research Institute
National Research Centre
Giza 12622, Egypt

The ORCID identification number(s) for the author(s) of this article can be found under https://doi.org/10.1002/admt.202401763

DOI: 10.1002/admt.202401763

and polymers was previously used but is lacking the retention of the functionality of the polymer and leads to highly crosslinked brittle films. Also, the metal nanoparticles size and composition are hardly tailorable as they form on the polymer surface.[4,5] Vapor phase techniques to deposit a polymer matrix with retained functionality could be molecular layer deposition (MLD) or Parylene CVD. However, MLD has limited deposition rates[6] and Parylene CVD can have aging limitations and creates precursors of very high temperatures of more than 500 °C making a codeposition setup complicated.[7–9] Initiated Chemical Vapor Deposition (iCVD) is best used in the low nano- to low micro-scale range as desired for nanocomposite thin film applications.[10] iCVD, as a version of hot wire CVD, uses resistive heating of wires inside a vacuum reactor to a temperature of just 150–400 °C. At these temperatures, only initiators are decomposed into radicals, while monomers preserve their full functionality.[11] A cooled sample stage around room temperature then promotes the adsorption of the gas phase species, leading to a highly surface-conformal radical polymerization even on thermally fragile substrates.[12–15] This makes iCVD perhaps the most attractive candidate for precisely tailored surface functionalities via polymer thin film coatings at the industrial scale,[16,17] with a growing palette of possible monomers that can be combined on demand.[18–22]

A nowadays already established way to precisely tailor the deposition of functional nanoparticles in the gas phase is a gas-aggregation cluster source (GAS).

In a GAS a target material is brought to the gas phase via DC magnetron sputtering from a metallic target, and nanoparticles form via nucleation, growth, coalescence, and coagulation while being transported by a gas flow toward an orifice which leads to a lower pressure chamber. By varying parameters and target materials the nanoparticle size, the size distribution or their composition can be tuned.[23–27]

In this work, iCVD of a polymer thin film is combined with the deposition of nanoparticles via a GAS in a single vacuum reactor for the first time. This enables the combination of an iCVD polytetrafluoroethylene (PTFE) thin film with silver nanoparticles (Ag NPs) resulting in a nanocomposite thin film. The analysis of the gas phase via mass spectrometry and the PTFE polymer chemistry via X-ray photoelectron spectroscopy (XPS) reveals, that unlike previous works in the combination of these materials[3–5] a well-defined polymer structure of the thin film can be preserved.

As especially in the biomedical area precisely tailored surface properties and functionalities are of huge interest[28–31] the nanocomposites were tested in antibacterial, antiviral, and anticancer applications. For this purpose, the impact of the Ag NPs in the nanocomposite was tested on *Enterococcus faecalis* bacteria, viruses including adenoviruses type 5 and SARS-CoV-2 as well as cancer cells while being compared to pure iCVD PTFE without Ag nanoparticles.

2. Results and Discussion

2.1. Codeposition Reactor for Nanocomposites

The codeposition reactor for polymer thin films containing nanoparticles was built by combining a GAS with an iCVD reactor as displayed in **Figure 1**. A ring inlet around the filaments was used for the precursors according to Schröder et al.[32] When the GAS nanoparticle deposition and the iCVD thin film deposition are operated simultaneously the high Ar gas flow of the GAS of 8 sccm inhibits the iCVD thin film deposition rate by more than 90% and results in far more nanoparticle volume fraction than polymer film volume fraction. Therefore, a microcontroller (Arduino) was used to control the power of the magnetron power supply and the gas flow rate via the mass flow controller (MFC) for the Ar flow in chosen time intervals. For nanocomposite deposition, the Ar gas flow rate is switching between a low flow rate of 1 sccm sufficient to hinder iCVD monomers and radicals from entering the GAS, and a high flow rate of 8 sccm required for the nanoparticle deposition when the plasma is activated. To sufficiently enclose the nanoparticles, which typically have a diameter of ≈10 nm, within the polymer film the low flow rate interval of 1 sccm was chosen to lead to ≈50 nm thickness. Different thicknesses and with that different filling factors can be created based on simply longer iCVD deposition times.

To investigate the influence of low and high Ar gas flow rates as well as the possible monomer molecule activation by the magnetron plasma in situ quadrupole mass spectrometry was used as described by Schröder et al.[33] where the individual molecules present are identified. The mass spectrometer (MS) was attached to the GAS+iCVD system displayed in Figure 1. The mass spectrum is displayed in **Figure 2a** with detailed peaks displayed in Figure 2b–g. The CF_2 peak at 50 m/z can clearly be identified, showing that the main building block of the polymer is present in the vapor phase in all situations. The Ar peak at 40 m/z can be seen in Figure 2d as expected, highest for 8 sccm gas flow and lowest for 1 sccm gas flow, with the active plasma possibly ionizing Ar and the magnetron accelerating them toward the target in the GAS. For the CO (2c)), FCO (2e)) and CF_3 (2f)) molecules the dilution by Ar flows leads to lower amounts. The F peak at 19 m/z in Figure 2b is the only peak decreasing by the additional plasma ignition at 8 sccm. This might indicate interactions of the precursors or their fragments with charged nanoparticles entering the iCVD chamber.[34]

As the GAS+iCVD codeposition reactor in Figure 1 is the first of its kind, the nanoparticles from the GAS were analyzed to see if the pressure of 40 Pa of the iCVD reactor changes the nanoparticle deposition drastically, as traditionally way lower pressures are used in the main chamber for a GAS. In Figure 2h a scanning electron micrograph of the resulting silver nanoparticles from the deposition without iCVD precursor flows but including filament power can be seen. The Micrograph was used to determine the particle distribution of more than 300 particles via the software "imagej" approximating round particles. As seen in Figure 2i the nanoparticles have an average diameter of 9.3 nm and follow a Gaussian size distribution.

2.2. Nanocomposite Analysis

The thickness of the codeposited PTFE+Ag sample of 185 ± 3 nm was analyzed by profilometry (Bruker, DektakXT). The nanoparticle size distribution seen in Figure 2i was used to estimate the nanoparticle filling factor of 0.08% via their volume. The nanocomposite was further investigated regarding its

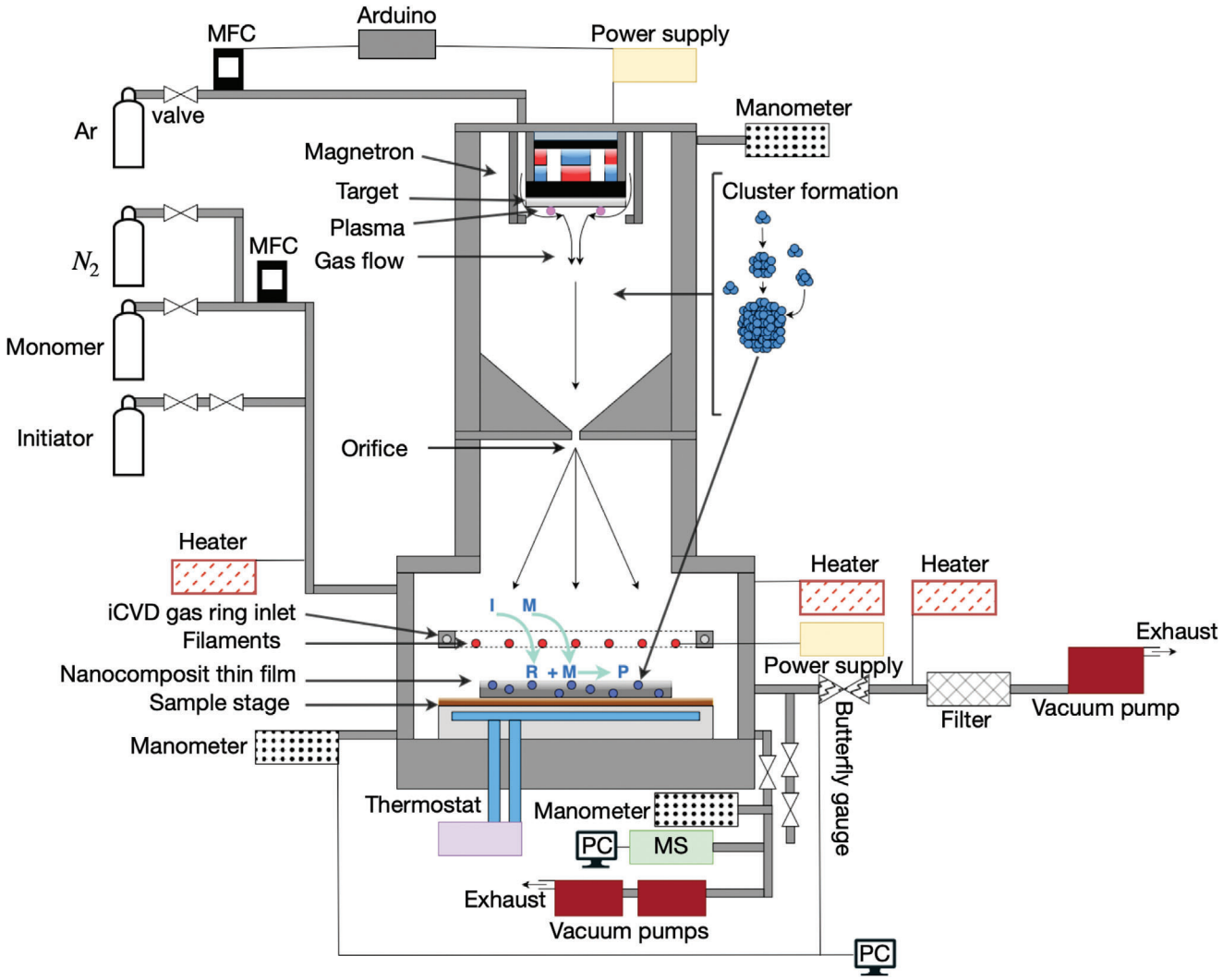

Figure 1. Schematic for the GAS+iCVD reactor used in the codeposition setup of iCVD PTFE thin film and GAS silver nanoparticles.

wetting behavior. The water contact angles (WCAs) show significant differences between the tested materials. In **Figure 3a** the WCAs of pure Ag nanoparticles of 61° ± 2°, 98° ± 4° for the nanocomposite, and 146° ± 20° for the pure iCVD PTFE thin film can be seen. As the coverage for the Ag nanoparticles is far below one monolayer, the WCA is probably dominated by the Si-wafer substrate. For the high WCA of the PTFE thin film the scanning electron micrograph, as seen in Supporting Information, reveals a complex surface topography previously reported by Chen et al. for fluoropolymers deposited via iCVD.[35] This topography does not occur for the nanocomposite as for the chosen parameters possibly the Ag NPs negatively impact the growth of the structures. As both polymer chemistries are the same, the impact on the following bio-interface performances of the rough surface topography of the thin film is expected to increase the antibacterial-, antiviral- and anticancer performance according to literature.[36–38] Hence, a higher performance of the lower roughness nanocomposite in these areas compared to the higher roughness PTFE thin film can be attributed to the Ag NPs.

In Figure 3b the XPS spectrum of the C1s peak of the nanocomposite can be seen. Compared to previous PVD-CVD-combinations[3,5] to codeposit PTFE and Ag a much more sophisticated polymer structure can be noticed. Only the CF_2 and C—C peaks are present which confirms a clear PTFE structure. The UV–VIS in Figure 3c confirms the Ag NPs in the nanocomposite due to the visibly higher absorption via plasmon resonance for wavelengths from 400 to 750 nm. In Figure 3d Fourier-transformed infrared spectroscopy (FTIR) was used to analyze the functional groups of the composite compared to the pure iCVD PTFE thin film. The deposition of nanoparticles via GAS does not result in a lack of functional groups in the nanocomposite as the CF_2 symmetrical and asymmetrical stretch are present at ≈1112 and 1181 cm^{-1} in both films. The portion of the asymmetrical CF_2 stretch in the nanocomposite is lower than in the PTFE thin film. The CF_2 symmetrical and asymmetrical stretch are macromolecular features.[39] The asymmetrical structure seems to be reduced due to the presence of the Ag nanoparticles within the nanocomposite. This could indicate a difference in crystalline structure within the

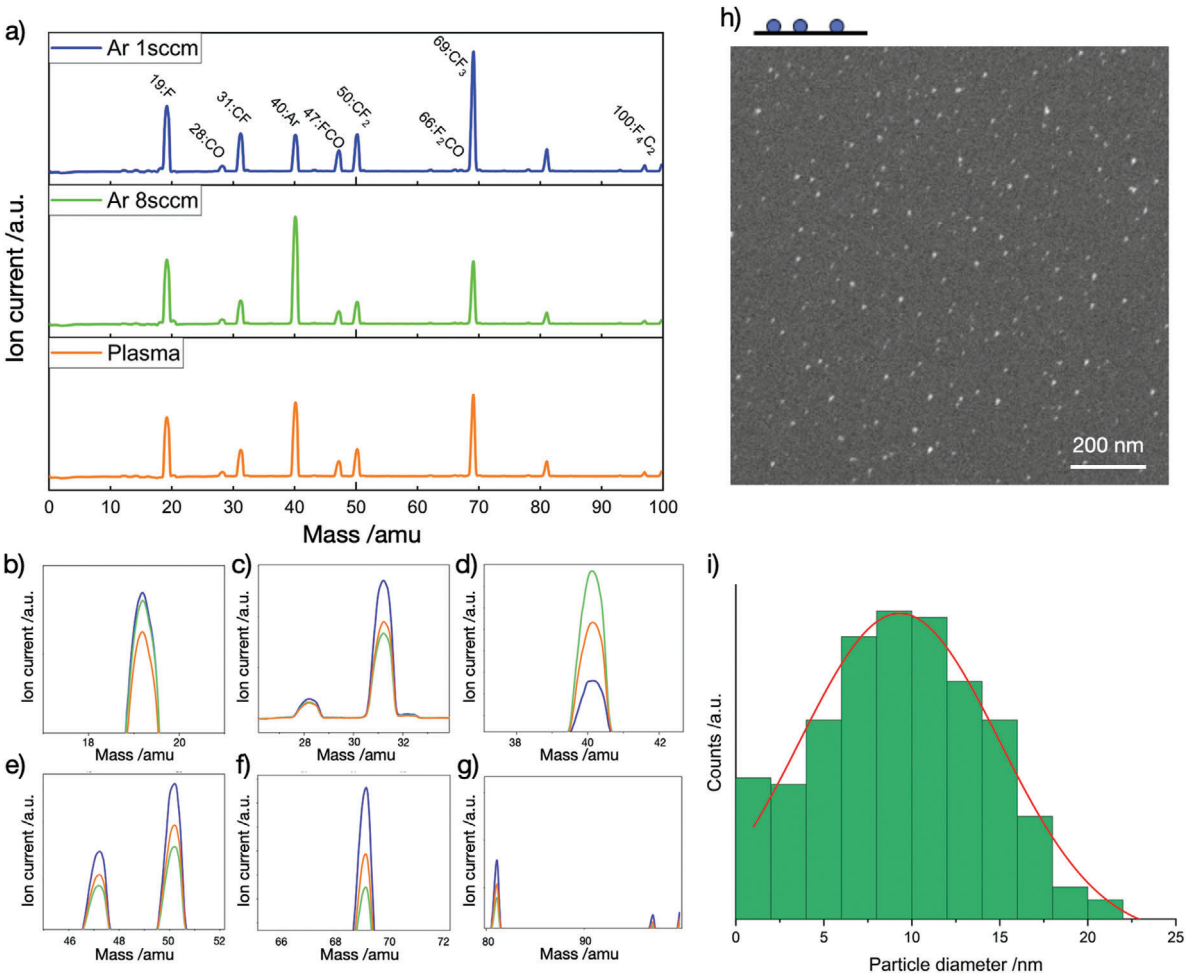

Figure 2. Chemical analysis of the gas phase and deposited materials. In a) the mass spectrum of the gas phase components during the deposition under 1 sccm Ar-flow, 8 sccm Ar-flow and 8 sccm Ar-flow + active plasma can be seen. The subpeaks are represented in b) for F, c) for CO and CF, d) for Ar, e) for FCO and CF_2, and g) for CF_3. In h) the scanning electron micrograph of the deposition of silver nanoparticles can be seen. The distribution of the particle diameter in i) reveals a normal distribution.

nanocomposite compared to the pure PTFE thin film via iCVD. This difference in macromolecular structure could be the reason no crystalline topography-features[35] are present on the surface for the nanocomposite as seen in Figure S2 (Supporting Information) compared to the crystalline features observed for the PTFE film.

2.3. Bio-Interface Performance

In the following, a wide scan of possible bio-interface use cases of the nanocomposite is tested compared to the pure Ag NPs and the pure PTFE thin film. The key results are presented in **Figure** 4 and discussed in the following sections.

2.3.1. Biocompatibility

The results of the cell viability tests via MTT can be seen in Figure 4a with additional information in Figure S1 (Supporting Information). For cell viability of human fibroblasts, the compared samples are all biocompatible as seen in Figure 4a) and do not differ significantly, while filopodial connections and cell-to-cell interactions were observed in all groups.

To conduct antiviral examinations with the materials, the viability of respiratory virus-affected cells first must be tested. For this VERO monkey kidney cells and VERO E6 cells, as seen in Figure S1 (Supporting Information), were tested. Results showed that all samples were biocompatible with no notable differences. As the materials do not impact the healthy cells in a negative way this allows to test the materials for antiviral properties against respiratory viruses Adenovirus-5 and SARS-CoV-2.

Further results showed that all tested materials were toxic on cancer cells with viability ranging from 15% to 46% on HepG2 liver cancer cells and from 49 to 53% on MCF-7 breast cancer cells as seen in Figures 4b and S1 (Supporting Information). As the results were more evident on HepG2 cells, further studies were conducted on the mechanism of the antiproliferative behavior against the liver cancer cells on a transcriptional level for some apopototic gene expressions.

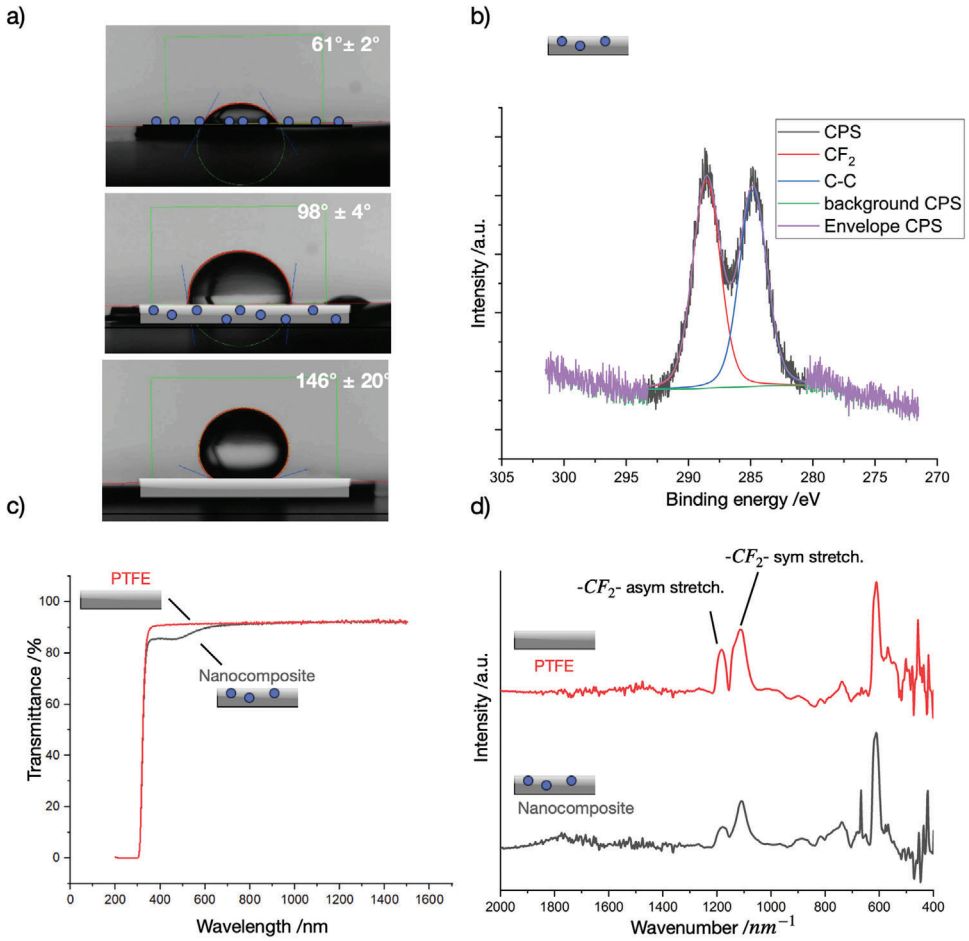

Figure 3. In a) the water contact angle of the Ag NPs, the nanocomposite, of the PTFE thin film are presented. In b) the C1s high-resolution XPS spectrum of the codeposited nanocomposite is shown. c) UV–vis spectroscopy results of the PTFE+Ag nanocomposite compared to pure iCVD PTFE. In figure d) the FTIR of the polymer thin film and nanocomposite are shown.

2.3.2. Antibacterial Behavior

The bacterial growth was determined in colony-forming units (CFU) using *Enterococcus faecalis* as seen in Figure 4c. The number of colony-forming *Enterococcus faecalis* species was 1.23×10^6 CFU mL^{-1} in the PTFE group, $1{,}33 \times 10^6$ CFU/ml in the Ag nanoparticles group, and $0{,}76 \times 10^6$ CFU mL^{-1} in the nanocomposite group, respectively. The assessment of the bacterial colonization via SEM (S1) revealed the conglomerate formation in Ag and PTFE groups, whereas the nanocomposite group showed overall single-bacterial adhesions. Despite the increase in hydrophobicity of the pure PTFE thin film, the reduced bacterial colonization in the nanocomposite group can be attributed to the antimicrobial characteristics of the Ag nanoparticles as commonly described in the literature.[40] The increased bacterial colonization and superior fibroblastic activity in the Ag group could be explained by the high hydrophilicity of the surface. Infections and stent thrombosis are the main problems in vascular surgery.[41]

Within the last two decades, drug-eluting stents have become an effective therapy strategy to reduce the incidence of restenosis. However, it has been proclaimed that the drug-eluting stents could inhibit the growth of endothelial cells, which are required to cover the vascular stent to reduce an excessive inflammatory response and could increase the risk of thrombosis.[42] Thus, there is a need for improved devices with enhanced effectiveness and physiological compatibility toward endothelial cells. Despite the need for further cytocompatibility studies with different cell lines and experimental models[43] and assessment of the corrosion resistance, their superior resistance against bacterial colonization without impairing fibroblastic activity could allow the speculation that deposition of the nanocomposites might be a promising strategy for clinicians dealing with thrombotic complications in vascular surgery.[44]

2.3.3. Antiviral Behavior

Regarding Adenovirus-5 the viral adsorption as well as virucidal mechanisms were examined using vero cells to test for antiviral behavior and its adsorption and virucidal mechanisms. The results are presented in Figure 4d,e, Tables S2,S3, and Figure S1 (Supporting Information). The viral control is marked as "positive cells" while the positive is a standard positive on a low level which is only used to validate the assay. For the PTFE thin films,

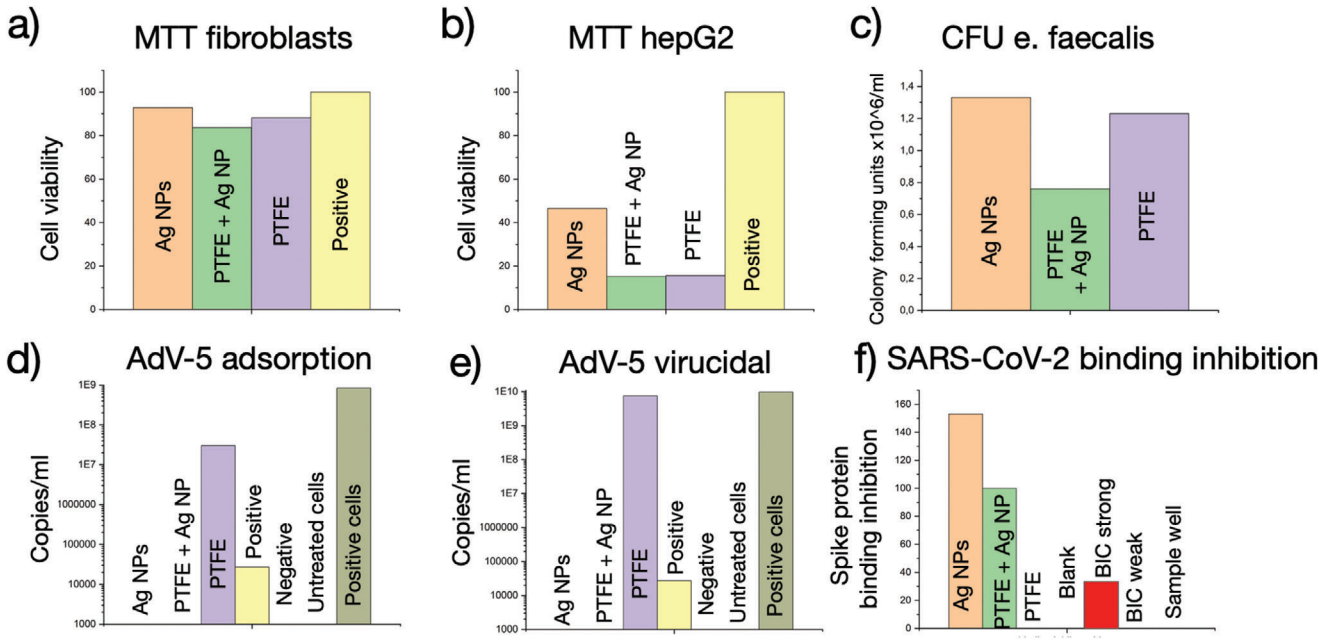

Figure 4. Presented is a wide scan of possible bio-interface use cases. Cell viability tests can be seen in a) for human fibroblasts and b) for HepG2 human liver cancer cells. In c) an analysis of colony-forming units (CFU) of *Enterococcus faecalis* bacteria on the sample's surface can be seen. In d) and e) antiviral analyses can be seen in copies/ml for Adenovirus 5 adsorption and virucidal analysis. In f) the binding inhibition toward the spike protein of SARS-CoV-2 via *covidrop* can be seen. Further analysis including anticancer behavior can be found in Tables S1–S6 (Supporting Information).

no antiviral activity was observed as the copies/ml even exceeded the positive control, while the PTFE + Ag NP nanocomposite's results were under the detection limit indicating antiviral behavior in both mechanistic ways.

Regarding antiviral activity against SARS-CoV-2 the ligand binding of the materials with the spike protein was examined using a *covidrop* ELISA assay. The results can be seen in Figure 4f, Figures S4 and S1 (Supporting Information). Ag NPs and the nanocomposite showed an inhibitory effect against the spike protein of SARS-CoV2 while the PTFE thin film showed no activity. A possible mechanism would be in the silver nanoparticles adsorbing on the virus surface which leads to local transformations of the surface, such as agglutination of glycoproteins, preventing the virus penetration into the cell.[45]

2.3.4. Mechanism of Anti-Proliferative Behavior Against HepG2 Liver Cancer Cells

The results for apoptotic gene expression on the mRNA level for HepG2 liver cancer cells can be found in Tables S5 and S6 as well as Figure S1 (Supporting Information). After 1 day the impact of the thin films is not distinct. After 4 days for the PTFE + Ag NP nanocomposite film the mRNA expression levels of caspase 3 and Bax genes were upregulated, indicating an apoptotic effect via the intrinsic pathway while BCL2 was downregulated indicating reduced anti-apoptotic behavior. All effects are stronger for the nanocomposite compared to the PTFE thin film.

Compared to the chemotherapy medication Paclitaxel the upregulation of apoptotic Caspase3 and Bax was weaker but the downregulation of anti-apoptotic BCL2 was stronger. The comparably rapid BCL2 downregulation of the Ag NPs after 1 day indicates the longer downregulation of the nanocomposite resulting from the functional silver nanoparticles.

3. Conclusion

The codeposition method of GAS+iCVD was successfully used to deposit PTFE matrix-Ag nanoparticle nanocomposite films via deposition in a single vacuum reactor. The mass spectrometry confirmed functioning initiated Chemical Vapor Deposition during the process, while the XPS and FTIR analysis confirmed a well-defined polymer structure of PTFE which was not reached before in such nanocomposites. Regarding antibacterial applications, the results demonstrate that the nanocomposite showed a higher resistance toward bacterial adhesion and biocolonization without significantly impairing the biocompatibility of the human fibroblasts. In contrast to the pure PTFE thin film the nanocomposite including Ag NPs showed antiviral behavior against the respiratory virus Adenovirus-5 via viral adsorption mechanisms and virucidal mechanisms. Against SARS-CoV-2 the nanocomposite also showed antiviral activity indicating possible applications.[45,46]

Regarding anticancer applications, the nanocomposite increased the apoptotic behavior compared to the pure thin film while even outdoing the chemotherapy medication paclitaxel in the decrease of one anti-apoptotic pathway via BCL2. Further analysis is needed for other gene expressions to build a more comprehensive understanding of the material's anticancer behavior. The new GAS+iCVD method enables the combination of the two worlds of precisely tailored polymer thin films via iCVD and functional nanoparticles via GAS, providing new pathways

for the fabrication of functional nanocomposites. The results presented in this paper, inter alia, pave the way for nanocomposites with an active, stimuli-sensitive polymer matrix.

4. Experimental Section

Gas Phase Deposition of PTFE Thin Film, PTFE + Ag Nanocomposite and Ag Nanoparticles: The used chemicals were PFBSF (perfluorobutanesulfonyl fluoride, 95%, Fluorochem, UK) and HFPO (hexafluoropropylene oxide, 97%, Fluorochem, UK).

PTFE Thin Films: PTFE thin films were deposited for 3 h by an HFPO (room temperature) gas flow of 0.5 sccm controlled by a mass flow controller (MC series, Alicat Scientific Inc., Tucson, AZ, USA) and a PFBSF (room temperature) gas flow of 0.1 sccm. The sample temperature was 20 °C and the pressure 50 Pa. A filament power of 70 W was applied. The Argon flow through the GAS was controlled by a mass flow controller (MCV series, Alicat Scientific Inc., Tucson, AZ, USA) and the magnetron power was controlled by a power supply (ADVANCED ENERGY, MDX 500). To ensure reproducibility the magnetron power supply and mass flow controller were operated via a microcontroller (Arduino Uno, custom microcode).

PTFE + Ag NPs Nanocomposite Films: The nanocomposite films were deposited for 3 h and 3 min. The HFPO (room temperature) flow was 0.5 sccm and the PFBSF (room temperature) flow 0.1 sccm. The sample temperature was 20 °C and the pressure 50 Pa. A filament power of 70 W was applied. The GAS was only used every 30 mins (6 cycles) for a magnetron time of 30 s at 100 W power. During the off-time, the Ar gas flow through the GAS was 1 sscm to prevent polymerization inside. During the on-time, the Ar gas flow was 8 sccm. During the magnetron on-time and 8 sccm Ar flow the iCVD process is naturally inhibited.

Ag NPs: For comparison samples with 6 cycles of 30 s magnetron on-time with 5 min off-time in between with the same parameters as in the PTFE + Ag NPs run were deposited without the flow of monomer and initiator and with 70 W filament power at 50 Pa.

Material Characterization: To investigate the successful codeposition of the combined GAS+iCVD setup mass spectrometry was used to analyze the iCVD process under the influence of Ar flow from the GAS and the plasma of the GAS. An open ion source quadrupole mass spectrometer (PrismaPlus, Pfeiffer Vacuum) was connected to the exhaust of the codeposition reactor as seen in Figure 1. For the different chosen reactor parameters of iCVD with and without the GAS Faraday scans were conducted from 1 to 100 amu with a scan time of 200 ms amu^{-1}.

To analyze a possible effect of nanoparticles and the surface topography on wetting water contact angle measurement was conducted on iCVD PTFE, GAS Ag nanoparticles, and the GAS+iCVD nanocomposite. The water contact angles were measured with a self-built measurement setup via the sessile drop technique with 5 µL deionized water droplets. The syringe was controlled by a step motor.

To investigate the surface chemistry of the GAS+iCVD nanocomposite thin film, X-ray photoelectron spectroscopy (XPS, XPS UHV system manufactured by PREVAC Sp. z o. o., Al-anode, 300 W) was utilized. Wide spectrum was obtained by scanning at 3 iterations and a pass energy of 200 eV, while high-resolution scans were performed at 20 iterations and a pass energy of 50 eV. The CasaXPS software (version 2.3.25) was used for the subsequent analysis of the XPS spectra. First, the Shirley function was used to model the background of each spectrum. Then, all relevant photoemission peaks were fitted using the asymmetric Lorentzian (LA) line shape, which is the convolution of the Lorentzian function with the Gaussian function. The charge correction was done by energy calibration of C 1s main peak. The measured C 1s main peak was set to the reference peak position of 284.8 eV. After energy calibration of C 1s peak, all relevant spectra were corrected by the same amount of the energy shift.

The UV–vis spectra were measured with a Perkin Elmer Lambda 900 from 200 to 1600 nm wavelength.

To investigate the surface roughness for the GAS+iCVD nanocomposite an atomic force microscope (SPM SmartSPM-1000, AIST-NT/ TESPA, NanoWorld) was used. The measured data was processed using Gwyddion software to determine the root mean square roughness of a 5 µm x 5 µm area, as seen in Figure S2 (Supporting Information).

Bio-Interface Performance Measurements—Bacterial Contamination: Cultivation with 10 mL sterile nutrient solution (BHI, Brain–Heart-Infusion Broth, Carl Roth GmbH + Co. KG, Karlsruhe, Germany) and 100 µL bacterial culture with E. faecalis (ATCC 29212) was conducted at 37 °C for 24 h. (Heraeus B6060, Heraeus Holding GmbH, Hanau, Germany). On the first day, the samples were infected with 200 mL of sterile BHI and 100 µL of the overnight culture and then incubated at 37 °C (Scientific C24 Incubator Shaker, New Brunswick Scientific, Edison, New Jersey, USA). After 4 h, the optical density was controlled via a spectrophotometer (BioPhotometer 6131, Eppendorf AG, Hamburg, Germany) at 600 nm (OD600), which was set to 0.8. The nutrient solution was exchanged every 24 h with 200 mL of sterile BHI for 6 days.

Bio-Interface Performance Measurements—Colony Forming Units (CFU): Each sample was placed in an Eppendorf tube containing 1 mL of sterile NaCl solution. To de-attach the bacteria from the surface, the samples were placed in an ultrasonic bath (ultrasonic bath Branson 2210R-MT Ultrasonic Cleaner, Branson Ultrasonics Corporation, Danbury/CT, USA) for 20 min. The bacterial suspension was then diluted to 10^{-2} and later to 10^{-4}. Afterward, the different dilution levels were applied to Caso agar plates. These Caso agar plates (CASO-Agar Ph.Eur., Carl Roth GmbH + Co. KG, Karlsruhe, Germany) were placed in an incubator at 37 °C (Heraeus B6060 incubator, Heraeus Holding GmbH, Hanau, Germany). After 24 h, the colony-forming units were counted with the germ counter (Germ counter BZG 25 from WTW, Xylem Analytics Germany Sales GmbH & Co. KG, Weilheim, Germany)

Bio-Interface Performance Measurements—Scanning Electron Microscopy of Bacteria: The samples were washed for 1 min with PBS (phosphate-buffered saline solution, Dulbeco, Biochrom GmbH, Berlin, Germany) and later with 1 ml of 4% glutaraldehyde. Afterward, the samples were washed three times for 5 min each time with PBS. The dehydration was carried out by means of an ascending series of 30%, 50%, 70%, 90% and 100% ethanol. The plates were then air-dried until ethanol had completely evaporated and attached to SEM sample plates (Agar Scientific Ltd, Stansted, Essex, United Kingdom) and stored overnight in a desiccator (Erich Eydam KG, Kiel, Germany). Gold sputtering with a thickness of 5 nm (BAL-TEC SCD 500, Leica Microsystems GmbH, Wetzlar, Germany) and examination using a scanning electron microscope (Philips XL 30 ESEM, Philips GmbH Market DACH, Hamburg, Germany) has been performed.

Bio-Interface Performance Measurements—Cytocompatibility: The experiments were performed after receiving approval from The Ethics Committee of the Medical Faculty of Christian Albrechts University, Kiel, Germany. (D640/20) and were conducted according to the guidelines of the Helsinki Declaration of Human Rights. Human fibroblasts were obtained from patients who had undergone oral surgical interventions such as tooth extraction third molar removal, etc. at the Oral and Maxillofacial Surgery Department at the Christian Albrechts University Hospital Schleswig-Holstein, Kiel Campus, Kiel, Germany. To prepare the time-dependent eluates, plates were incubated for 30 min, 8, h and 24 h in the corresponding medium in order to dissolve potentially cytotoxic substances. After the first day of cell culture, eluate samples were obtained and the MTT-Test was carried out on cell dilution series after 5 days. Cell proliferation was assessed by using the MTT Cell Proliferation Kit (#11465007001, Roche Diagnostics, Mannheim, Germany). 96-well microtiter plates with 5×10^3 cells per well were incubated for 24 h and a sample of 100 µL eluate was obtained. After an incubation period of 24 h, cell proliferation was measured. The optical density of the samples was measured photometrically at 450 nm wavelength. As a positive control, cells were cultivated on a bare glass plate.

Cytotoxicity on HepG2 Cells (Human Liver Cancer Cells), MCF-7 (Human Breast Cancer Cells), Vero Cells and Vero E6 Cells Using MTT Assay: The cytotoxic effect of the studied materials against proliferation of human liver cancer cells (HepG2) and human breast cancer cells (MCF-7) was performed using an MTT colorimetric assay. All results were compared with paclitaxel as a positive control which is used as a conventional cancer

treatment. All materials were tested with vero cells (monkey kidney cells) as a normal control to prove anti-proliferative activity against cancer cells.

These experiments were performed by seeding vero cells into a 24-well plate on the first day, then incubating for 24 h at 5% CO2 incubator. On the second day the cells were treated with the materials (Ag nanoparticles, PTFE, and PTFE + Ag nanocomposite), after exposure to UV for 20 min on each side for sterilization and again incubated for 48 h. On the fourth day 200 µL of MTT dye was added and incubated for 3 h to allow the formation of crystals, then 1000 µL of dimethyl sulfoxide was added. The data was analyzed using GraphPad Prism version 6 software.

Before testing the antiviral activity, the cytotoxicity of the proposed materials was determined using an (MTT) assay with 3-(4,5-dimethylthiazol-2-yl)-2,5-diphenyltetrazolium bromide on Vero and Vero E6 cell lines. The assay is based on the solubilization of formazan crystals which were formed by MTT dye and solubilized by dimethyl sulfoxide. The measurements were conducted at 570 nm using a microplate reader (CLARIOstar Plus, BMG LABTECH, Germany).

Apoptotic Effect of the Tested Materials Against Human Liver Cancer Using Quantitative Real-Time PCR Assay: The cells were seeded at a density of 500 000 cells per well into six well plates. On the second day, the plates were treated with the materials and incubated. After 1 or 4 days the cells were harvested, washed with phosphate buffer saline, subjected to trypsinization, and the pellet was frozen at -80 until assessed by quantitative real-time PCR.

Nucleic Acid Extraction: A Gene Jet RNA purification kit (Thermo Scientific, Inc, USA) was used for total RNA extraction according to the manufacturer's instructions. The first-strand cDNA was synthesized using oligodT primers and the RevertAid Reverse Transcriptase kit (Thermo Scientific, USA).

Quantitative Real-Time PCR (Q-PCR): Q-PCR was performed for the detection of expression levels of Caspase 3, BCl2, and BAX genes. GAPDH was used as a housekeeping gene (internal control). The PCR cocktail was composed of 12.5 µL SYBR Green reagent (Thermo Scientific, USA), 2 µL synthesized cDNA, 3 µL of each primer of Caspase-3, bcl2, and BAX genes also, GAPDH, and 4.5 µL of molecular grade water in a total volume of 25 µL. Q-PCR was run by a quantitative real-time detection system (Applied Biosystems 7500 Fast Real-Time PCR system Thermal Cycling Block, USA). The amplification was performed under the following conditions: 1 min at 95 °C, 40 cycles of 95 °C for 1 min, 58 °C for 1 min, and 72 °C for 2 min. The post-amplification melting temperature (Tm) analysis, clearly differentiated nonspecific PCR products. Negative controls (Non-template water instead of cDNA) were also included to ensure the lack of reagent DNA contamination.

The Q-PCR data was analyzed using the comparative CT method.[47] Briefly, the difference in cycle threshold, ΔCT, was determined as the difference between the tested gene and human GAPDH. ΔΔCT was obtained by the difference between the two groups. The fold change (FC) was calculated as $2^{-\Delta\Delta CT}$.

Antiviral Assay Against Human Adenovirus Type 5 (Virucidal and Adsorption Mechanisms): Vero cells were seeded into a six-well plate (5 × 105 cells per well), then incubated for 24 h at 5% CO2 incubator.

To examine the virucidal antiviral mechanism on the second day Adenovirus type 5 (human respiratory model) was prepared at 1/100 dilution (TCID50 is 106), then each material was incubated with 0.5 mL of prepared virus and 0.5 plain media with the proposed material at 4 °C for 1 h, the cells were infected by 1 mL per each well and 1 mL maintenance medium was added. After incubation for 24 h the CPE (cytopathic effect) was displayed in the viral control and a quantitative PCR assay was performed.

To examine the viral adsorption antiviral mechanism, on the second day the cells were treated with the materials, incubated for 24 h, and on the third day the cells were infected by the virus 1/100 as previously mentioned. 200 µL in each well were incubated for 1 h at 37 °C in a 5% CO_2 incubator with shaking every 15 min. Afterward, they were discarded and put in a maintenance medium and subsequently incubated for 24 h in the CO_2 incubator.

The results were obtained once the CPE was displayed under the inverted microscope to verify antiviral activity compared with viral and cell controls. Viral copies were determined using a quantitative real-time PCR assay after freezing and thawing the plates 3 times.

Antiviral Assay Against SARS-CoV2 Using CoviDrop SARS-CoV-2 Spike-ACE2 Binding Inhibitor Screening Assay: Anti-SARS-CoV-2 tests were carried out using CoviDrop SARS-CoV-2 Spike-ACE2 Binding Inhibitor Screening Fast Kit (EpiGentek, USA). The entry of SARS-CoV-2 into human host cells occurs through the binding of surface unit S1 of its spike protein to the cell receptor angiotensin-converting enzyme 2 (ACE2).

Therefore, the method is based on pre-coating SARS-CoV-2 spike protein onto microplate wells. His-tagged ACE2 was bound to the coated spike protein in the presence or absence of inhibitors. The amount of the bound ACE2, which was proportional to the ACE2 inhibition intensity, was then recognized by the Binding Detection Solution containing anti-His antibody and measured through an ELISA-like reaction by reading the absorbance in a microplate spectrophotometer at a wavelength of 450 nm. The binding activity of ACE2 was proportional to the optical density intensity measured. The more the ACE2 binding was inhibited, the lower the OD intensity was. Methods were carried out according to the manufacturer's instructions.

The Binding Inhibition is Calculated as

$$\text{BindingInhibition\%} = [1 - (\text{InhibitorSampleOD} - \text{BlankOD}/\text{NoInhibitorSampleOD} - \text{BlankOD})] \times 100\% \quad (1)$$

Supporting Information

Supporting Information is available from the Wiley Online Library or from the author.

Acknowledgements

The authors would like to thank the German Research Foundation for funding through the RTG 2154 (project number 270394294) via project P4, the SFB 1261 (project number 286471992) via project A2 and KiNSIS (Kiel Nano, Surface and Interface Science). The authors also acknowledge partial funding of this research through the German Federal Government via the ZIM project "Clean Window" KK5010203WZ1. A.A. would like to thank DAAD for her funded scholarship at Kiel University under the supervision of F.F.

Open access funding enabled and organized by Projekt DEAL.

Conflict of Interest

The authors declare no conflict of interest.

Data Availability Statement

The data that support the findings of this study are available from the corresponding author upon reasonable request.

Keywords

antibacterial, antiviral, cancers, codeposition, gas aggregation cluster source, initiated chemical vapor deposition

Received: October 18, 2024
Revised: January 14, 2025
Published online: February 8, 2025

[1] A. Balazs, T. Emrick, T. Russell, *Science* **2006**, *314*, 1107.

[2] G. Schmidt, M. Malwitz, *Curr. Opin. Colloid Interface Sci.* **2003**, *8*, 103.
[3] F. Faupel, V. Zaporojtchenko, T. Strunskus, M. Elbari, *Adv. Eng. Mater.* **2010**, *12*, 1177.
[4] V. Zaporojtchenko, V. Chakravadhanula, F. Faupel, S. Tamalevicius, M. Andrulevicius, A. Tamuleviciene, L. Augulis, *Thin Solid Films* **2010**, *518*, 5944.
[5] U. Schürmann, W. Hartung, H. Takele, V. Zaporojtchenko, F. Faupel, *Nanotechnology* **2005**, *16*, 8.
[6] S. George, *Chem. Rev.* **2010**, *110*, 111.
[7] K. Achyutan, P. Sawyer, G. Mata, G. White, R. Bernstein, Sandia National Lab (SAND2014-17853), **2014**.
[8] P. Moni, A. Al-Obeidi, K. Gleason, *Beilstein J. Nanotechnol.* **2017**, *8*, 723.
[9] C. Tan, H. Craighead, *Materials* **2010**, *3*, 1803.
[10] K. Gleason, *Adv. Mater.* **2024**, *36*, 2306665.
[11] R. Bakker, V. Verlaan, A. Verkerk, C. van der Werf, L. van Dijk, H. Rudolph, J. Rath, R. Schropp, *Thin Solid Films* **2009**, *517*, 3555.
[12] K. Gleason, *CVD polymers: Fabrication of Organic Surfaces and Devices*, John Wiley & Sons, Hoboken, NJ, USA **2015**.
[13] K. Gleason, *Nat. Rev. Phys.* **2020**, *2*, 347.
[14] K. Lau, *CVD polymers: Fabrication of Organic Surfaces and Devices*, John Wiley & Sons, Hoboken, NJ, USA **2015**.
[15] S. Baxamusa, S. Im, K. Gleason, *Phys. Chem. Chem. Phys.* **2009**, *11*, 5227.
[16] K. Yilmaz, H. Sakalak, M. Gürsoy, M. Karaman, *Ind. Eng. Chem. Res.* **2019**, *58*, 14795.
[17] H. Sakalak, K. Yilmaz, M. Gürsoy, M. Karaman, *Chem. Eng. Sci.* **2020**, *215*, 115466.
[18] V. Graur, A. Mukherjee, K. Sebakhy, R. Bose, *Polymers* **2022**, *14*, 3993.
[19] M. Burk, S. Schröder, W. Moormann, D. Langbehn, T. Strunskus, S. Rehders, R. Herges, F. Faupel, *Macromolecules* **2020**, *53*, 1164.
[20] P. Materna, D. Illek, K. Unger, M. Thonhofer, T. Wrodnigg, A. Coclite, *Monatsh Chem.* **2023**, *154*, 544.
[21] K. Lau, K. Gleason, *Thin Solid Films* **2008**, *516*, 678.
[22] T. Hartig, A. Mohamed, N. Fattah, A. Gülses, T. Tjardts, E. Kangah, K. Chan, S. Veziroglu, Y. Acil, O. Aktas, J. Wiltfang, S. Loutfy, T. Strunskus, F. Faupel, A. Amin, S. Schröder, *Adv. Mater. Interfaces* **2023**, *11*, 2300587.
[23] H. Haberland, M. Karrais, M. Mall, Y. Thurner, *J. Vac. Sci. Technol. A* **1992**, *10*, 3266.
[24] V. Popok, O. Kylian, *Applied Nano* **2020**, *1*, 4.
[25] D. Nikitin, J. Hanus, S. Ali-Ogly, O. Polonskyi, J. Drewes, F. Faupel, H. Biederman, A. Choukorov, *Plasma Processes Polym.* **2019**, *16*, 1900079.
[26] A. Bahl, J. Strobel, W. Reichstein, O. Polonskyi, T. Strunskus, L. Kienle, F. Faupel, *Nanotechnology* **2017**, *28*, 175703.
[27] J. Drewes, N. Perdana, K. Rogall, T. Hartig, M. Elis, U. Schürmann, F. Pohl, M. Abdelaziz, T. Strunskus, L. Kienle, M. Elbahri, F. Faupel, C. Rockstuhl, A. Vahl, *Part. Syst. Charact.* **2023**, *41*, 2300102.
[28] R. Yang, K. Gleason, *Langmuir* **2012**, *28*, 12266.
[29] W. Reichstein, L. Sommer, S. Veziroglu, S. Sayin, S. Schröder, Y. Mishra, E. Saygili, F. Karayürek, Y. Acil, J. Wiltfang, A. G. F. Faupel, O. Actas, *Polymers* **2021**, *13*, 186.
[30] A. Khlyustova, Y. Cheng, R. Yang, *J. Chem. B* **2020**, *8*, 6588.
[31] J. Lahann, *Polym. Int.* **2006**, *55*, 1361.
[32] S. Schröder, T. Strunskus, S. Rehders, K. Gleason, F. Faupel, *Sci. Rep.* **2019**, *9*, 2237.
[33] S. Schröder, A. Hinz, T. Strunskus, F. Faupel, *J. Phys. Chem. A* **2021**, *125*, 1661.
[34] J. Kousal, O. Polonskyi, O. Kylian, A. Choukourov, A. Artemenko, J. Pesicka, D. Slavinska, H. Biederman, *Vacuum* **2013**, *96*, 32.
[35] Z. Chen, T. Nguyen, S. Rumrill, K. Lau, *Adv. Mater. Interfaces* **2022**, *9*, 2101961.
[36] K. Menzies, L. Jones, *Optom. Vis. Sci.* **2010**, *87*, 387.
[37] U. Eduok, J. Szpunar, E. Ebenso, *Prog. Org. Coat.* **2019**, *137*, 245.
[38] F. Dawson, W. Yew, B. Orme, C. Markwell, R. Ledesma-Aguilar, J. Perry, I. Shortman, D. Smith, H. Torun, G. Wells, M. Unthank, *Langmuir* **2022**, *38*, 10632.
[39] J. Piwowarczyk, R. Jedrzejewski, D. Moszynski, K. Kwiatkowski, A. Niemczyk, J. Baranowska, *Polymers* **2019**, *11*, 1629.
[40] N. Duran, M. Duran, M. Bispo de Jesus, A. Seabra, W. Favaro, G. Nakazato, *Nanomed. Nanotechnol. Biol. Med.* **2016**, *12*, 789.
[41] S. Del Pace, M. Boddi, R. Rasoini, S. Micheli, C. Alderighi, S. Caciolli, M. Margheri, R. Abbate, G. Gensini, *Intern. Emerg. Med.* **2010**, *5*, 121.
[42] N. Bassous, J. Cooke, T. Webster, *Methodist Debakey Cardiovasc. J.* **2016**,*12*, 163.
[43] N. Abbasnezhad, M. Shirinbayan, S. Champmartin, F. Bakir, *J. Biomech.* **2023**, *146*, 111425.
[44] A. Haidar, A. Ali, S. Veziroglu, J. Fiutowski, H. Eichler, I. Müller, K. Kiefer, F. Faupel, M. Bischoff, M. Veith, O. Aktas, H. Abdul-Khaliq, *Nanoscale Adv.* **2019**, *1*, 4659.
[45] C. Weiss, M. Carriere, L. Fusco, I. Capua, J. Regla-Nava, M. Pasquali, J. Scott, F. Vitale, M. Unal, C. Mattevi, D. Bedognetti, A. Merkoci, E. Tasciotti, A. Yilmazer, Y. Gogotsi, F. Stellacci, L. Delogu, *ACS Nano* **2020**, *14*, 6383.
[46] F. Zabihi, J. Reissner, A. Friese, M. Schulze, C. Nie, P. Nickl, L. Lehmann, P. Siller, C. Melcher, T. Schneiders, T. Gries, U. Rösler, R. Haag, *Adv. Mater. Technol.* **2023**, *8*, 2300141.
[47] T. Schmittgen, K. Livak, *Nat. Protoc.* **2008**, *3*, 1101.